Syntheses, structures and redox properties of some complexes containing the Os(dppe)Cp* fragment, including [Os(dppe)Cp*2(μ-C[triple bond, length as m-dash]CC[triple bond, length as m-dash]C)]

Michael I. Bruce, Karine Costuas, Thomas Davin, Jean-François Halet, Kathy A. Kramarczuk, Paul J. Low, Brian K. Nicholson, Gary J. Perkins, Rachel L. Roberts, Brian W. Skelton, et al.

Syntheses, structures and redox properties of some complexes containing the Os(dppe)Cp* fragment, including [{Os(dppe)Cp*}$_2$(μ-C≡CC≡C)]†‡

Michael I. Bruce,*[a] Karine Costuas,[b] Thomas Davin,[b] Jean-François Halet,[b] Kathy A. Kramarczuk,[a] Paul J. Low,*[c] Brian K. Nicholson,[d] Gary J. Perkins,[a] Rachel L. Roberts,[c] Brian W. Skelton,[e] Mark E. Smith[c] and Allan H. White[e]

Received 7th August 2007, Accepted 21st September 2007
First published as an Advance Article on the web 11th October 2007
DOI: 10.1039/b712104k

The sequential conversion of [OsBr(cod)Cp*] (**9**) to [OsBr(dppe)Cp*] (**10**), [Os(=C=CH$_2$)(dppe)Cp*]PF$_6$ ([**11**]PF$_6$), [Os(C≡CH)(dppe)Cp*] (**12**), [{Os(dppe)Cp*}$_2${μ-(=C=CH–CH=C=)}][PF$_6$]$_2$ ([**13**](PF$_6$)$_2$) and finally [{Os(dppe)Cp*}$_2$(μ-C≡CC≡C)] (**14**) has been used to make the third member of the triad [{M(dppe)Cp*}$_2$(μ-C≡CC≡C)] (M = Fe, Ru, Os). The molecular structures of [**11**]PF$_6$, **12** and **14**, together with those of the related osmium complexes [Os(NCMe)(dppe)Cp*]PF$_6$ ([**15**]PF$_6$) and [Os(C≡CPh)(dppe)Cp*] (**16**), have been determined by single-crystal X-ray diffraction studies. Comparison of the redox properties of **14** with those of its iron and ruthenium congeners shows that the first oxidation potential E^1 varies as: Fe ≈ Os < Ru. Whereas the Fe complex has been shown to undergo three sequential 1-electron oxidation processes within conventional electrochemical solvent windows, the Ru and Os compounds undergo no fewer than four sequential oxidation events giving rise to a five-membered series of redox related complexes [{M(dppe)Cp*}$_2$(μ-C$_4$)]$^{n+}$ (n = 0, 1, 2, 3 and 4), the osmium derivatives being obtained at considerably lower potentials than the ruthenium analogues. These results are complimented by DFT and DT DFT calculations.

Introduction

Contemporary interest in molecules containing unsaturated carbon chains linking transition metal–ligand groups[1,2] has resulted in much work centred on complexes of the type {L$_x$M}(C≡C)$_n${ML$_x$} (n = 1–14), containing end-groups such as Pt(PR$_3$)$_2$(Ar),[3] MnI(dmpe)$_2$,[4] Mn(dmpe)(η^5-C$_5$H$_4$Me),[5] Mn(C≡CSiR$_3$)(dmpe)$_2$,[6] Re(NO)(PPh$_3$)Cp*,[7] Fe(CO)$_2$Cp*,[8] Fe(PP)Cp* (PP = dppe, dippe)[9,10] and Ru(PP)Cp′ [PP = (PPh$_3$)(PR$_3$), R = Me, Ph; dppm, dppe; Cp′ = Cp, Cp*],[11] many of which have been demonstrated to undergo several step-wise one-electron oxidations. Their electronic structures have attracted attention, with theoretical calculations showing that the HOMOs of these complexes generally have both metal and carbon character, the relative amounts of which depend on the length of the carbon chain and the nature of the end-groups.[12–14] Consequently, oxidation of these species can involve removal of electrons from orbitals which are delocalised over all atoms of the M–(C≡C)$_n$–M bridge,[7,11] or from orbitals localised predominantly either on the carbon chain itself (as in the Mn complexes[4–6]) or at the metal centres (for Fe).[9,10]

The magnetic properties of these redox-active complexes are directly linked to their electronic structures and are of considerable interest. With the exception of the Mn derived series,[4] all neutral M–C$_4$–M species described to date are diamagnetic and best described in terms of a buta-1,3-diyne-1,4-diyl structure (*i.e.*, the limiting valence structure **A**, Scheme 1).[9] In the case of the manganese complexes, magnetic susceptibility measurements suggest a triplet ground state for the neutral complex [{*trans*-MnI(dmpe)$_2$}$_2$(μ-C≡CC≡C)] (*i.e.*, a neutral diradical with formal d^5–d^5 configurations at each Mn centre), although it should be noted that this 34-electron complex offers two fewer electrons than the other 36-electron buta-1,3-diynediyl complexes. Sequential one-electron oxidations of [{*trans*-MnI(dmpe)$_2$}$_2$(μ-C≡CC≡C)] lead to mono- and di-cations with doublet and singlet electronic structures, respectively, with the Mn centres capping an increasingly cumulenic carbon fragment.[4] Similar observations have been made on other members of the family of Mn$_2$C$_4$ complexes.[6]

The product derived from one-electron oxidation of [{Fe(dppe)Cp*}$_2$(μ-C≡CC≡C)] (**1**; **A**, Scheme 1) also has a buta-1,3-diynediyl structure with the radical sites localised on the metal centres (structures **B** and **C**).[9] The paramagnetic dication [**1**]$^{2+}$ has a singlet (**D**)–triplet (**E**) energy gap sufficiently small (ΔG_{ST} = −18.2 cm^{-1}) for both states to be populated, even at liquid nitrogen temperatures. Removal of a third electron from the Fe–C$_4$–Fe substructure is also possible, the use of the very electron-donating and bulky dippe ligand allowing isolation of

[a]*School of Chemistry and Physics, University of Adelaide, Adelaide, South Australia, 5005, Australia*
[b]*Laboratoire des Sciences Chimiques de Rennes, UMR 6226 CNRS-Université de Rennes 1, F-35042, Rennes, Cedex, France*
[c]*Department of Chemistry, University of Durham, South Road, Durham, UK DH1 3LE. E-mail: p.j.low@durham.ac.uk; Fax: + 44 191 384 4737*
[d]*Department of Chemistry, University of Waikato, Hamilton, New Zealand*
[e]*Chemistry M313, SBBCS, University of Western Australia, Crawley, Western Australia, 6009, Australia*

† Dedicated to Professor Ken Wade, on the occasion of his 75th birthday, and in celebration of his remarkable career.

‡ CCDC reference numbers 617825–617829. For crystallographic data in CIF or other electronic format see DOI: 10.1039/b712104k

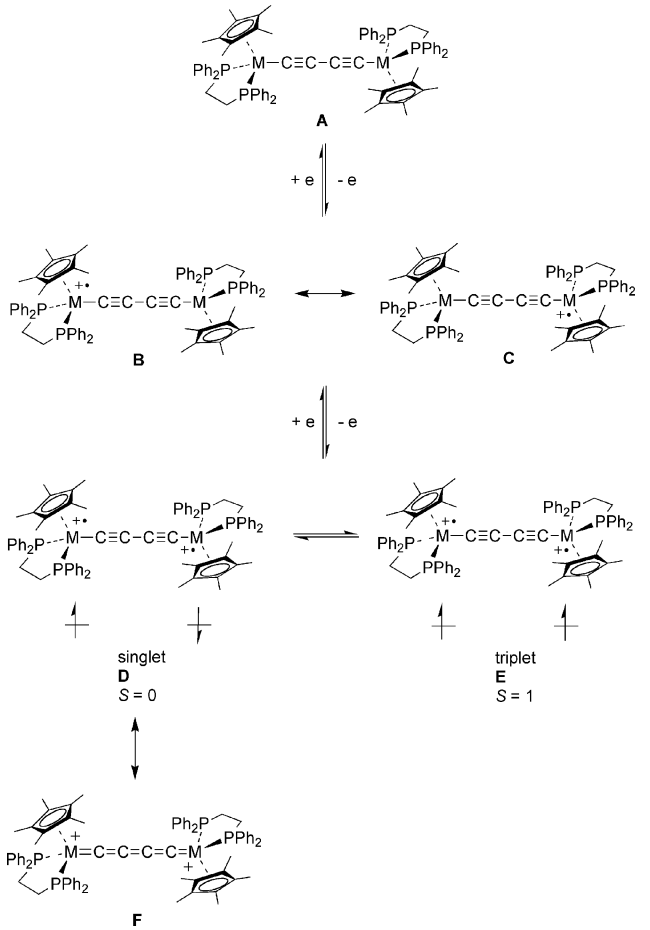

Scheme 1 Representations of the oxidation processes and products derived from buta-1,3-diynediyl complexes [{M(dppe)Cp*}$_2$(μ-C≡CC≡C)].

[{Fe(dippe)Cp*}$_2$(μ-C$_4$)](PF$_6$)$_3$ ([**5**](PF$_6$)$_3$), which is a three-spin carrier at 293 K.[10]

Various spectroscopic, structural and computational studies show a smooth transition from the buta-1,3-diynediyl structure of the diruthenium complexes [{Ru(PP)Cp′}$_2$(μ-C≡CC≡C)] [Cp′ = Cp, PP = (PPh$_3$)$_2$ **2**; Cp′ = Cp*, PP = dppe **3**] (**G**, Scheme 2) to the cumulenic structure **H** in the derived dications and eventually to the acetylide-bridged dicarbyne **I** in the tetracations.[11] Similar observations have been made for the rhenium complexes [{Re(NO)(PPh$_3$)Cp*}$_2$(μ-C$_4$)]$^{n+}$ ([**4**]$^{n+}$, n = 0–2), although no dirhenium system of this type has yet been oxidised beyond the dication.[4] In contrast to the iron species [**1**]$^{2+}$, the dicationic ruthenium and rhenium complexes [**2**]$^{2+}$, [**3**]$^{2+}$ and [**4**]$^{2+}$ have been reported to be diamagnetic between 80 and 300 K.[7,11]

The families of complexes derived from **1** and **3** feature the same ligand environment about metal centres from the same periodic Group, yet differ in terms of the number of accessible oxidation states and their electronic and magnetic structures. Given these structural similarities, the observed differences in magnetic and electronic behaviour for the iron and ruthenium complexes suggest that it is the metal termini which play a decisive role in dictating the nature of the spin-carriers and their interactions, therefore underpinning the long-range magnetic and electronic interactions between them.

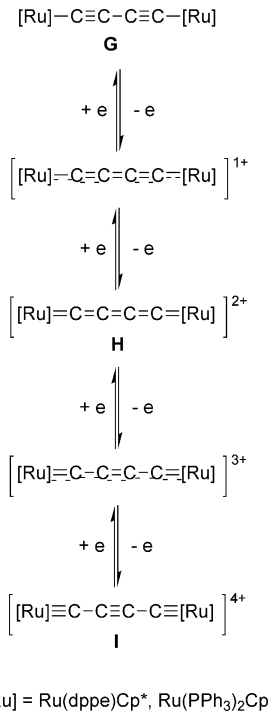

Scheme 2 Oxidation processes of compounds **2** and **3**. Similar structures are appropriate for the oxidation of **4**.

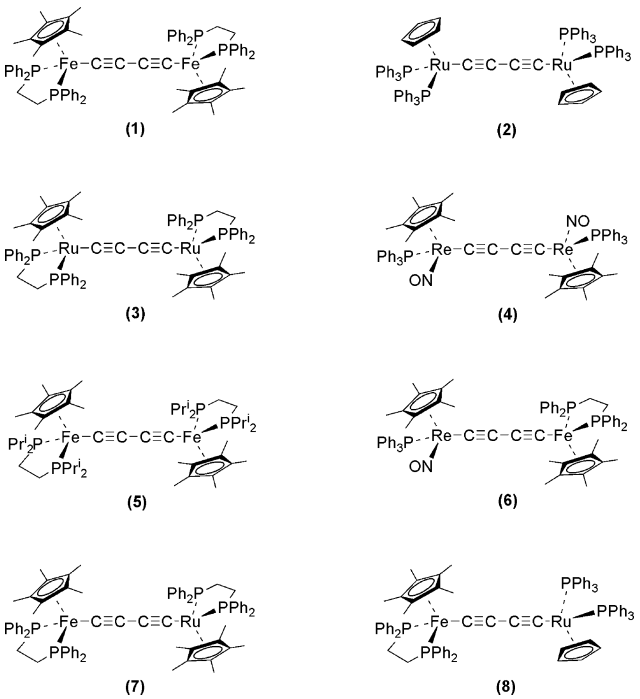

A detailed study of the hetero-bimetallic complexes [{Cp*(dppe)Fe}C≡CC≡C{Ru(dppe)Cp*}] (**7**) and [{Cp*(dppe)-Fe}C≡CC≡C{Ru(PPh$_3$)$_2$Cp}] (**8**), which undergo step-wise oxidation with [FeCp$_2$]PF$_6$ to give the mono- and di-cations, [**7**](PF$_6$)$_n$ and [**8**](PF$_6$)$_n$ (n = 1, 2), has also been reported.[15] Computational work indicates these systems possess delocalised electronic structures, with a significant contribution from the iron centre to the highest lying orbitals. This description is supported

by the available X-ray structural data, together with the IR spectrum of **[8]**$(PF_6)_2$, which shows a decrease in the ν(CC) frequency, and which are consistent with the gradual evolution of the polycarbon moiety from a diynediyl structure to a more cumulenic system as oxidation proceeds. These data, together with ^{57}Fe Mössbauer, ESR, IR, UV-vis and NIR spectra allow an estimation of the relative contributions of the metal centres and ancillary ligands to the properties of the $[\{ML_x\}(\mu\text{-}C_4)\{M'L_x\}]^{n+}$ assemblies and clearly indicate the dominant role of ruthenium over iron in dictating the underlying electronic structures of C_4-bridged bimetallic complexes.

To date, there has been no example of a series of buta-1,3-diynediyl complexes containing the metals of a triad with the same ligand environments. In many cases, this has resulted from difficulties in obtaining such a series, the extensive studies of compounds containing the Re(NO)(PPh_3)Cp* end-groups[7] not being replicated for Mn (this ligand environment has not yet been accessed) or Tc (because of its radioactive character). Even with the Group 8 elements, where studies of the chemistry of Ru$(PPh_3)_2$Cp complexes are common, some of which have been duplicated with osmium, the Fe$(PPh_3)_2$Cp group is apparently too sterically congested to be capable of isolation. However, with a smaller, chelating diphosphine, such as dppe, analogous complexes containing all three elements of Group 8 can be prepared. It is obviously of interest to examine the osmium complexes related to those described above to complete the picture of the changes attendant on descending the group and this paper describes some osmium complexes with the same ligand environment [Os(dppe)Cp*] as in the Fe and Ru complexes previously studied.[15]

Results

Syntheses

The conversion of OsO_4 to [OsBr(cod)Cp*] (**9**) and thence to [OsBr(dppe)Cp*] (**10**) was achieved by the sequence of reactions shown in Scheme 3. Reduction of OsO_4 by HBr to give H_2OsBr_6,[16] followed by reaction with Cp*H in ethanol may give any of three products, as described by Girolami and coworkers.[17] It is necessary to control reaction times carefully and to exclude oxygen to obtain the complex $[\{Os(\mu\text{-}Br)BrCp^*\}_2]$. Although this complex does not react with dppe to give [OsBr(dppe)Cp*], the latter could be

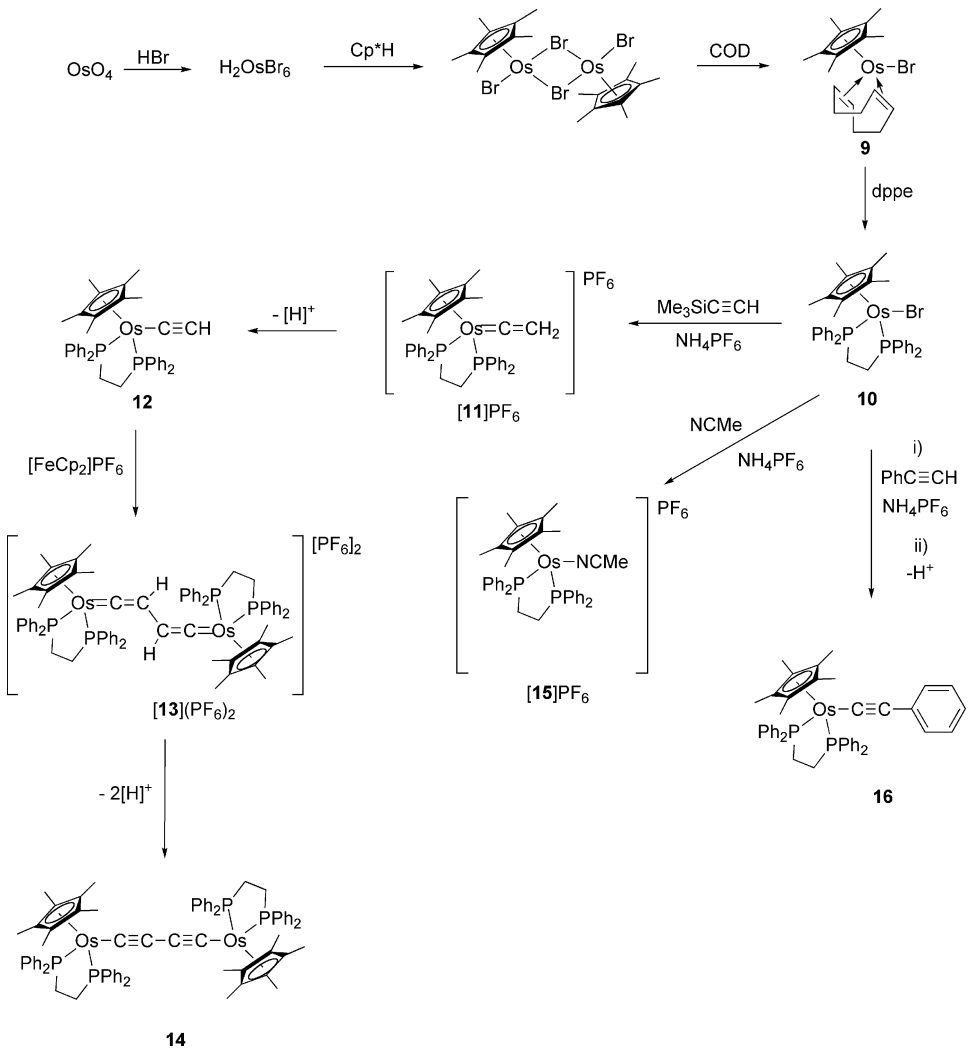

Scheme 3 The preparation of the homometallic osmium diynediyl complex **14**, associated intermediates and related compounds.

obtained *via* the reactive intermediate [OsBr(cod)Cp*], obtained from [{Os(μ-Br)BrCp*}$_2$] and 1,5-cyclooctadiene (cod).[17] More recently, we have developed methods for accessing these precursors from potassium osmate, $K_2[OsO_2(OH)_4]$, which provides a more convenient and less hazardous entry into organo-osmium chemistry.[18]

Regardless of the method of preparation of **9**, substitution of the labile cod with dppe in refluxing heptane led to the formation of **10** in high yield (81%). Complexes **9** and **10** were characterised by ^{1}H, ^{13}C and ^{31}P NMR spectroscopy along with ES-MS and elemental microanalyses. In the ^{1}H NMR spectra of **9** and **10**, singlet resonances at δ 1.61 and 1.68, respectively, arise from C_5Me_5. Multiplets between δ 1.71 and 4.07 are assigned to CH_2 and CH protons of the cod ligand in **9**, while for **10**, multiplets are found at δ 2.09 and 2.62 (CH_2) and at δ 6.97–7.92 (Ph). The ^{13}C NMR spectra of **9** and **10** contained resonances for Cp* at δ 9.51 and 9.82 (singlets, Me) and δ 85.12 and 94.01 [triplets, J(CP) 3 Hz, ring C], together with two singlets at δ 68.1 and 69.3 (cod in **9**) or multiplets centred at δ 30.77 (CH_2) and between δ 127.75–140.86 (Ph) (dppe in **10**). The ^{31}P resonance for the dppe ligand in **10** is at δ 43.0. The electrospray (ES) mass spectrum of **10** contained both the molecular ion at m/z 804, arising from in-source oxidation, and the Br-loss ion [Os(dppe)Cp*]$^+$ at m/z 725.

A reaction sequence utilising the coupling of metal acetylide radical cations was used to convert **10** to [{Cp*(dppe)Os}$_2$(μ-C≡CC≡C)] (**14**).[9a] There is a significant decrease in reactivity of **10** compared with the iron or ruthenium chloro analogues, so that the reaction between **10** and HC≡CSiMe$_3$ in the presence of $[NH_4]PF_6$ required extended heating (72 h). The vinylidene [Os(=C=CH$_2$)(dppe)Cp*]PF_6 ([**11**]PF_6) was isolated as a pale yellow powder in 90% yield. Vinylidene **11** was readily deprotonated with KOBu^t in thf to give the osmium ethynyl [Os(C≡CH)(dppe)Cp*] (**12**) as a yellow solid in 59% yield. The ethynyl complex **12** is very air-sensitive in solution, the reaction mixture turning deep green upon exposure to only traces of oxygen. Oxidative coupling of **12** with $[FeCp_2]PF_6$ afforded the (bis)vinylidene [{Cp*(dppe)Os}$_2${μ-(=C=CH–CH=C=)}]$(PF_6)_2$ ([**13**]$(PF_6)_2$) as a grey powder (68%), which was then deprotonated with KOBu^t to give the required diynediyl complex, [{Os(dppe)Cp*}$_2$(μ-C≡CC≡C)] (**14**) as a bright orange powder in 66% yield. In the presence of oxygen, the reaction mixture rapidly turns dark green, resulting in loss of product.

Complexes [**11**]PF_6, **12**, [**13**]$(PF_6)_2$ and **14** were characterised spectroscopically and all gave satisfactory elemental microanalyses. Thus, the IR spectra contained ν(CC) bands at 1633 ([**11**]PF_6), 1929 (**12**), 1611 ([**13**]$(PF_6)_2$) and 1965 cm^{-1} (**14**), consistent with the change in CC bond order as indicated in Scheme 3; other characteristic bands were at 836 ([**11**]PF_6), 841 ([**13**]$(PF_6)_2$ [ν(PF)] and 3274 cm^{-1} [**12**, ν(≡CH)]. In the ^{1}H NMR spectra, the Cp* groups gave singlets between δ_H 1.43–1.99 and δ_C 9.72–10.99 ($C_5\mathit{Me}_5$) and δ 88.59–92.17 (ring C). For **12**, the ring C resonance showed a triplet coupling to ^{31}P (3 Hz). In vinylidene complexes [**11**]PF_6 and [**13**]$(PF_6)_2$, the characteristic low-field resonances for C_α were at δ 305.27 and 309.69, respectively, with C_β resonating at δ 100.64 and 100.37. Phenyl resonances are found in the usual regions, between δ_H 6.74–7.99 and δ_C 127.0–140.0. In the alkynyl complex **12**, resonances for C_α and C_β are at δ 92.91 and 89.88, respectively, whilst those for the diynediyl complex **14** are observed at δ 71.32 (C_α) and 95.46 (C_β). In the neutral complexes, the ^{31}P resonance arising from the dppe ligand lies between δ 43.3 and 43.7, while in the cations, it is at δ 40.8 ([**11**]PF_6) or 39.5 ([**13**]$(PF_6)_2$). ES mass spectra contain parent ions or cations at the calculated m/z values.

Treatment of **14** with one equivalent of $[FeCp_2]PF_6$ in dichloromethane caused a rapid colour change from orange to deep green. The mono-cation [**14**]PF_6 was isolated by precipitation from the reaction mixture following addition of hexane. Not surprisingly, on account of the 35-electron configuration of the cation, the ^{1}H NMR spectrum of the product was broad and considerably paramagnetically shifted. Peaks at δ_H 12.16 (Cp*), 10.68 (CH_2) and multiplets at δ_H 7.36–8.22 (Ph) were assigned from their relative intensities. However, satisfactory ^{13}C and ^{31}P NMR spectra were not obtained. The IR spectrum contained ν(CC) at 1860 cm^{-1} (*cf.* [**3**]PF_6 ν(CC) 1859 cm^{-1}),[11b] corresponding to a decrease in the $C_\alpha C_\beta$ bond order. The ES mass spectrum contained M$^+$ at m/z 1496.

Oxidation of **14** with two equivalents of $[FeCp_2]PF_6$ in dichloromethane caused a rapid change in colour through the deep green of the mono-cation to a deep blue solution, from which the dicationic [**14**]$(PF_6)_2$ was isolated by precipitation with hexane as an analytically pure powder. The ^{1}H NMR spectrum of this 34-electron complex displayed well-resolved signals at δ 2.13 (Cp*), 3.19–3.31 and 3.58–3.69 (CH_2) and 6.99–7.80 (Ph), consistent with a diamagnetic complex. The diamagnetic character of [**14**]$(PF_6)_2$ is in agreement with geometry optimizations performed at the DFT level of theory on model [**14-H**]$^{2+}$ (see Computational details) which reveal that the low spin (LS) state is energetically favored by 18 kJ mol^{-1} over the high spin (HS) state. The same result was obtained for the ruthenium dication analogue, *i.e.*, the LS state is preferred over the HS state, but with an energy difference somewhat smaller (13 kJ mol^{-1}). The ^{31}P NMR spectrum contained a slightly broadened singlet at δ 81.0 (dppe) and a septet at δ −143.0 (PF_6). The dramatic shift of over 37 ppm in the dppe resonance is consistent with removal of electron density from the osmium centre upon oxidation. The IR spectrum contains ν(CC) at 1781 cm^{-1}, indicative of a further decrease in CC bond order towards the metallacumulenic structure. In the ES mass spectrum, the doubly-charged cation M^{2+} is found at m/z 748.

Two further derivatives of the Os(dppe)Cp* moiety were prepared to provide a larger set of reference compounds for comparative purposes. Replacement of Br by NCMe was achieved by heating **10** in acetonitrile in the presence of $[NH_4]PF_6$, which afforded [Os(NCMe)(dppe)Cp*]PF_6 ([**15**]PF_6) as an off-white powder in 74% yield. Characteristic spectral data include IR ν(CN) and ν(PF) bands at 2264 and 838 cm^{-1}, the Cp* resonances at δ_H 1.80 and δ_C 9.6 and 89.34 [Cp*; the latter a triplet with J(CP) 3 Hz] and 119.62 (CN) and δ_P 43.3 (dppe) and −143.7 (PF_6). The characteristic dppe resonance in the ^{31}P NMR spectrum is consistent with the formal 18-electron count at the metal centre. The molecular cation was at m/z 766 in the ES mass spectrum.

Reaction of **10** with HC≡CPh in ethanol gave an orange solution, which presumably contains the substituted vinylidene [Os(=C=CHPh)(dppe)Cp*]Br. This solution was cooled and treated with NaOEt to give the neutral alkynyl [Os(C≡CPh)(dppe)Cp*] (**16**) as a lemon-yellow powder in 83% yield. The IR spectrum of **16** was characterised by ν(CC) at 2085 cm^{-1}, whilst characteristic NMR resonances were observed at δ_H 1.68 and δ_C 10.00 and 89.19 for the Cp* ligand, and for

C_α and C_β at δ 105.99 and 97.04, respectively. The characteristic phosphine resonance at δ_P 43.7 ppm was also observed.

Molecular structures

The molecular structures of [**11**]PF_6, **12**, **14**, [**15**]PF_6 and **16** have been determined by single-crystal X-ray crystallography. Fig. 1–5 contain plots of single molecules or cations, while Tables 1–3 contain selected bond distances and angles and crystallographic refinement details. Compared with the extensive studies that are available for ruthenium, there have been relatively few structures of mononuclear complexes containing OsL_2Cp' (L = tertiary phosphine, Cp′ = Cp, Cp*) groups reported and only those of [OsX(dppe)Cp*] (X = Cl, Br),[18] [Os(=CH_2)(dppm)Cp*]OTf,[19] [Os{SiR_2(X)}(PMe_3)$_2$Cp*] (X = OTf, R = Me,[20] Pr^i;[21] X = Cl, R = Pr^i[21]), [Os(L)(PMe_3)$_2$Cp*]$^+$ (L = $SiMe_2$, $SiPr^i_2$),[21] [{Os(PMe_3)$_2$Cp*}$_2$(μ-LL)]$^{2+}$ (LL = N_2, S_2),[21] [Os(OTf)(dppm)Cp*][22] and [Os(OH_2)(dmpm)Cp*]$^{+}$[22] contain Cp* ligands. However, the similarity of the atomic radii of ruthenium (1.34 Å) and osmium (1.35 Å) suggests that there should be few structural differences between analogous complexes containing these metals.

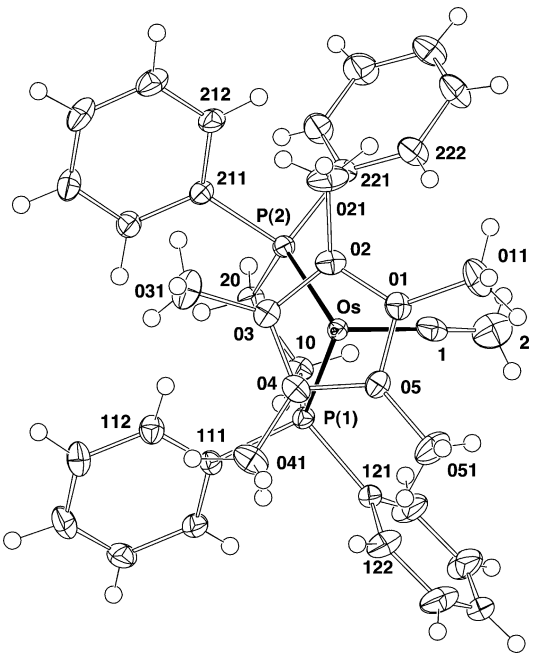

Fig. 1 A plot of the cation [Os(=C=CH_2)(dppe)Cp*]$^+$ in [**11**]PF_6 showing the atom labelling scheme.

The complexes described here all have the usual nearly octahedral geometry containing the Os(dppe)Cp* fragment, for which Os–P distances of between 2.2451(8) and 2.2752(9) Å are found for the neutral compounds, lengthening to between 2.2996(5) and 2.3151(6) Å in cations [**11**]$^+$ and [**15**]$^+$ as a consequence of the decreased Os–P back-bonding interactions. The Os–C(Cp*) distances are similar in all complexes, ranging between 2.224(3) and 2.328(3) Å (mean 2.26 Å). The corresponding values for analogous ruthenium complexes lie between 2.223 and 2.275(3) Å. The dppe ligands also have similar geometries in each case, with P–C distances between 1.833(3) and 1.872(7) Å and C–C separations averaging 1.52 Å. The pseudo-octahedral geometry about the Os atom is shown by the angles subtended by the non-Cp* ligands, with P–Os–P falling between 81.18 and 83.35(3)°, and P–Os–X between 80.3 and 91.43(8)°.

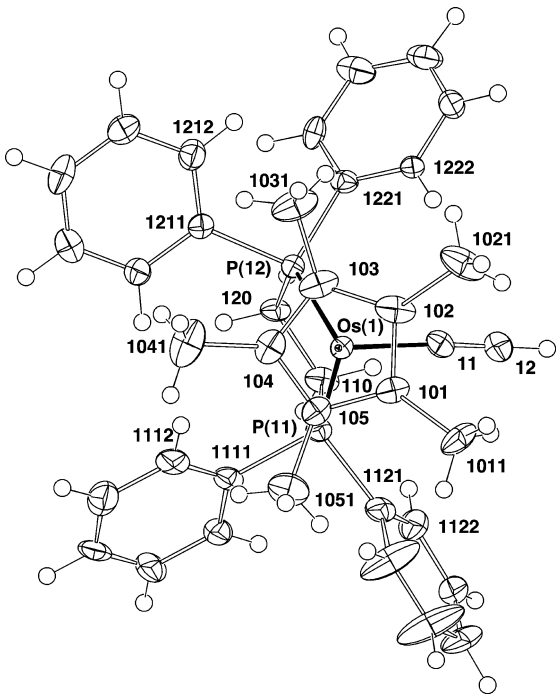

Fig. 2 A plot of a molecule of [Os(C≡CH)(dppe)Cp*] (**12**).

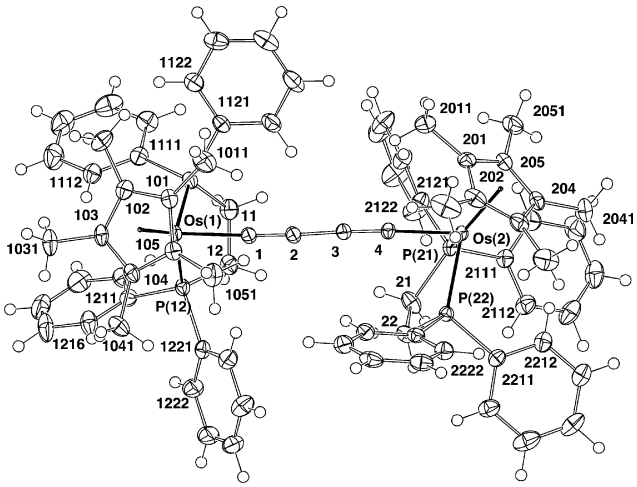

Fig. 3 A plot of a molecule of [{Os(dppe)Cp*}$_2$(μ-C≡CC≡C)] (**14**).

The Os–C distances reflect the nature of the carbon ligand. For vinylidene **11**, the Os=C bond length is 1.910(3) Å, consistent with the multiple bond character of this interaction; in contrast, the Os–C≡ distances in **12** and **16** lie between 2.012(3) and 2.043(8) Å. Within the carbon ligands, the formal C=C double bond in **11** is unusually short at 1.183(6) Å, albeit without libration correction, but on the basis of extensive data measured at 'low' temperatures, while the C≡C triple bonds in **12** and **16** are 1.16(1) and 1.202, 1.208(5) Å, respectively. Angles at C(1) are 175.4(3) (**11**), 174.4, 177.2(8) (**12**) and 174.4, 177.9(3)° (**16**), and 174.1, 176.6(3)° at C(2) in **16** (Table 1).

Table 1 Selected bond distances (Å) and angles (°) for some OsX(dppe)Cp* complexes

Complex	[**11**]PF_6·MeOH [X = C=CH_2]	**12** (molecules 1;2) [X = C≡CH] (molecules 1;2)	**14**·C_5H_{12}[a] [X = (–C≡C–)$_2$] Os(1;2)	[**15**]PF_6 [b] [X = NCMe]	**16**·0.25C_6H_6 [c] [X = C≡CPh] (molecules 1;2)
Os–P(1,2)	2.3081(8), 2.3151(6)	2.265, 2.263(2); 2.262, 2.258(2)	2.2583(9), 2.2515(9); 2.2451(8), 2.2548(9)	2.2999, 2.2996(5)	2.2625(7), 2.2682(8); 2.2721(8), 2.2752(9)
Os–C(cp)	2.262–2.328(3)	2.245–2.302(8); 2.235–2.274(7)	2.226–2.285(3); 2.224–2.279(3)	2.226–2.264(2)	2.236–2.274(3); 2.230–2.291(3)
(av.)	2.29(3)	2.27; 2.26(2)	2.26; 2.26(2)	2.245(13)	2.26; 2.26(2)
Os–C(1)	1.910(3)	2.017; 2.043(8)	2.010; 2.015(3)	2.028(2) [N(01)]	2.026; 2.012(3)
C(1)–C(2)	1.183(6)	1.16; 1.16(1)	1.220; 1.224(4)	1.128(3)[b]	1.202; 1.208(5)
C(2)–C(X)			1.380(4) [C(3)]	1.465(4) [C(02)]	1.443; 1.437(4) [C(21)]
P(1)–Os–P(2)	82.42(3)	82.68; 82.88(7)	81.18(3); 82.66(3)	82.41(2)	83.35, 83.35(3)
P(1)-Os-X	83.4(1)	80.3; 82.4(2)	81.79; 83.19(9)	88.89(4)	81.17; 81.62(8)
P(2)–Os–X	91.43(8)	90.4; 88.2(2)	84.72; 81.03(9)	84.82(4)	86.30; 87.16(9)
Os–C(1)–C(2)	175.4(3)	174.4(8); 177.2(7)	177.4; 177.2(3)		177.9; 174.4(3)
C(1)–C(2)–C(3)			176.2; 177.4(3)		

[a] Difference map residues were modelled in terms of a disordered C_5H_{12}; the compound is isomorphous with its hexane solvated ruthenium analogue.[11b] In the table read C(4, 3) as C(1, 2) for the parameters related to Os(2). [b] Os–N(01)–C(01) 177.4(2), N(01)–C(01)–C(02) 178.8(2)°. [c] C(1)–C(2)–C(21) 174.1, 176.6(3)°.

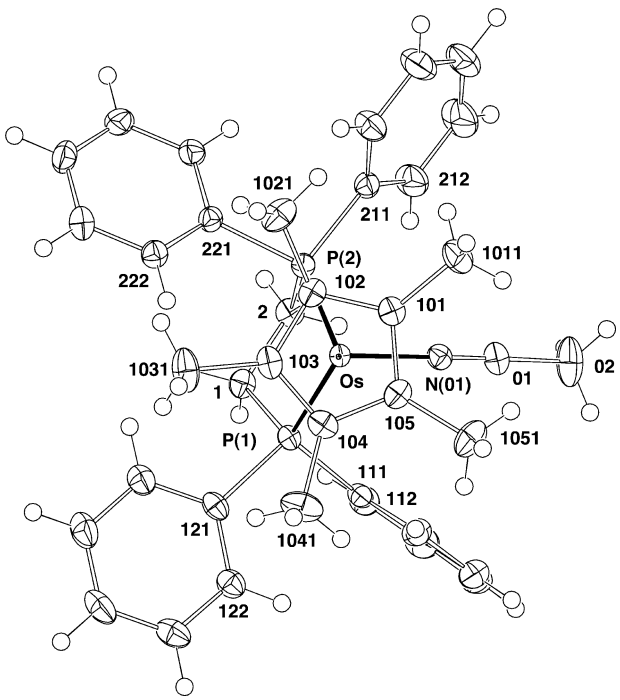

Fig. 4 A plot of the cation [Os(NCMe)(dppe)Cp*]$^+$ in [**15**]PF_6.

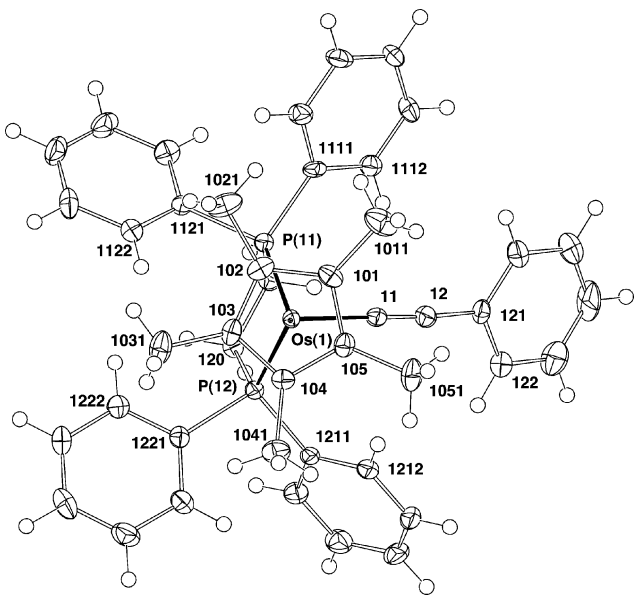

Fig. 5 A plot of a molecule of [Os(C≡CPh)(dppe)Cp*] (**16**).

Structural comparisons of {Cp*(dppe)M}$_2$(μ-C≡CC≡C) (M = Fe, Ru, Os)

The synthesis of **14** completes a triad of complexes for Group 8 metals with identical ligand environments. This provides the opportunity for a detailed comparison of their properties, although limited in this account to their spectroscopic properties and structural similarities in the M–C_4–M bridge, as other features are similar to those described above. Selected bond data for the three complexes are collected in Table 2. The structure of **14** as the pentane solvate is isomorphous with that of the corresponding hexane solvated ruthenium complex.[11b] In all three complexes, the two metal fragments adopt a non-centrosymmetric arrangement about the carbon chain, arising from rotation of the –CM(dppe)Cp* fragment about the C(2)–C(3) bond. Along the linear four-carbon bridging ligand, the carbon–carbon bond distances give rise to a short–long–short pattern consistent with the diynediyl structure, with the C≡C bonds being comparable for all three complexes and falling around 1.22 Å, whereas the central C–C bond is around 1.38 Å. These values show that the C–C bonds are shortened and the C≡C bonds are lengthened to approximately the same extent in all complexes, with respect to the C–C bond of ethane (1.532(2) Å)[23] and C≡C bond of ethyne (1.178(2) Å),[24] in turn suggesting a similar degree of electron delocalisation along the carbon chain is in effect in each case.

The data summarised in Table 2 show that there is slight departure from linearity in the M–C_4–M chains in the case of each of the three complexes **1**, **3** and **14**, with the angles at the C(sp) atoms lying in the range 175–179(1)°. A similar observation has

Table 2 Comparative structural data for [{Cp(dppe)M}$_2$(μ-C$_4$)](PF$_6$)$_n$ (M = Fe, Ru, Os; n = 0–2)

M	n	M–P(1;2)/Å	M–C(1)/Å	C(1)–C(2)/Å	C(2)–C(2′)/Å	M–C(1)–C(2)/°	C(1)–C(2)–C(2′)/°	Torsion Cp(0)···M···M′···Cp(0′)/°	M–Cp(0)[a]/Å	M···M/Å	Ref.
Fe	0	2.1687(10), 2.1692(8); 2.1634(8), 2.1723(11)	1.884; 1.889(3)	1.220; 1.221(4)	1.373(4)	178.9; 174.7(3)	176.8(3); 177.0(3)	−78.9	1.73_8; 1.73_7	7.564	12*b*
Fe	1	2.238(2); 2.206(2)	1.830(8)	1.236(9)	1.36(1)	167.0(6)	177(1)	169.9	1.76_6	7.431	9*a*
Ru	0	2.2556, 2.2420(8)	2.001,2.003(3)	1.223,1.218(4)	1.382(4)	176.6,177.1(3)	176.9,178.0(3)	−47.1	1.89_7,1.89_6	7.821	11*b*
Ru	1	2.2756, 2.3001(5)	1.931(2)	1.248(3)	1.338(3)	165.6(2)	178.0(2)	180	1.90_5	7.6293	11*b*
Ru	2	2.319, 2.312(1); 2.311,2.330(1)	1.858,1.856(5)	1.280,1.269(7)	1.294(7)	175.6,170.1(4)	176.7,174.2(6)	−40.1	1.91_9, 1.92_9	7.476	11*b*
Fe-Ru[b]	0	2.190, 2.201(1); 2.215, 2.197(1)	1.939(4); 1.957(4)	1.223(6); 1.233(6)	1.374(6)	177.3; 177.3(4)	176.6(4); 177.7(4)	47.1	1.81_1, 1.82_5	7.721	15
Fe-Ru	1	2.2360, 2.2680(6)	1.886(2)	1.240(3)	1.349(3)	166.1(2)	177.5(3)	180	1.83_2	7.636	15
Fe-Ru	2	2.239(7), 2.204(8); 2.396(11), 2.348(9)	1.881(7); 1.731(9)	1.261(5); 1.260(5)	1.325(5)	171.7(4); 169.2(4)	174.0(4)	−44.7	1.77_9, 1.77_2	7.536	15
Os (**14**)	0	2.2583, 2.2515(9); 2.2451(8), 2.2548(9)	2.010(3); 2.015(3)	1.220(4); 1.224(4)	1.380(4)	177.4(3); 177.2(3)	176.2(3); 177.4(3)	−47.4	1.90_5, 1.89_9	7.843	This work

[a] Cp(0) = centroid of Cp*. [b] Fe/Ru disordered, average values of M–X bonds cited.

been made for a number of other {ML$_x$}(μ-C$_n$){M′L$_x$} complexes, with the extent of "bending" becoming more pronounced in complexes with longer chains.[25] Though the reason for the non-linearity of the carbon chains in this kind of complex cannot be precisely determined in any particular example, we can assume that interactions with solvent molecules (if present), van der Waals, electrostatic or electronic π-type interactions are probably at work. Interestingly, DFT calculations performed on the Fe, Ru, and Os series in vacuum at 0 K show that a slight bending of a few degrees of the metal–carbon chain slightly stabilises the molecules (≤2 kJ mol^{-1}) over the linear form. This is due to a combination of small orbital and electrostatic interactions, which together sum to an observable effect.

As can be seen from the preceding discussion, the structures of the diynediyl complexes of Fe, Ru and Os are very similar. The only difference of note is the length of the M–C(1) bonds, the Fe–C(1) bond being significantly shorter [1.889(3) Å] than both the Ru–C(1) and Os–C(1) bonds [2.001(3) Å and 2.010(3) Å, respectively], arising from the different sizes of the metal centres.[26] The DFT optimized structural arrangements of the corresponding neutral model compounds show the same trend, *i.e.*, the Fe–C(1) bond length (1.917 Å) is, as expected, shorter than the Ru–C(1) and Os–C(1) distances, which are nearly equivalent (2.028 Å and 2.026 Å, respectively). Upon oxidation, the Os–C(1) bond is slightly more affected than the Ru–C(1) bond, with a contraction of 0.068 Å and 0.126 Å for the one and two-electron oxidation products, respectively, *vs.* contractions of 0.055 Å and 0.102 Å for the Ru series. The C(1)–C(2) bond lengths are virtually identical in the Ru and Os complexes, with the value in the dicationic osmium compound [**14-H**]$^{2+}$ only 0.004 Å longer than the ruthenium homologue.

Redox properties

The cyclic voltammogram of **14** was recorded (298 K, scan rate of 0.2 V s^{-1}; CH_2Cl_2 solution with 0.1 M [NBu$_4$]BF$_4$ as supporting electrolyte). Scans between −2.0 and +2.0 V contain four one-electron oxidation waves consistent with stepwise oxidation of the neutral diynediyl complex to the mono-, di-, tri- and tetra-cations (Table 4). The first three processes are fully reversible, with the fourth oxidation being partially chemically reversible. The redox processes are all well separated, with the differences in formal potentials, ΔE°, lying in the range 440 to 830 mV. The large values of ΔE° are an indication of the stability of the various redox products with respect to disproportionation under the conditions of the experiment.

Table 4 lists the half-wave potentials of **14**, along with the corresponding values from the analogous ruthenium[11*b*] and iron[9*a*,10] complexes under almost identical conditions. The potentials of **14**, whilst significantly lower than those of the ruthenium complex, are comparable to those of the iron complex, an interesting observation, since the oxidation potentials of the complex {Cp*(dppe)Fe}$_2$(μ-C≡CC≡C) are among the lowest for organometallic complexes of this type reported to date,[11*b*] with only the manganese complexes described by Berke being more readily oxidised.[4]

The DFT geometry optimisations performed for each oxidation state allow the calculation of the adiabatic ionisation potentials (*IP*) (Table 5). A rather good fit between experimental oxidation

Table 3 Crystal data and refinement details for complexes [**11**]PF_6, **12**, **14**, [**15**]PF_6 and **16**

Compound	[**11**]PF_6††	**12**	**14**‡‡	[**15**]PF_6	**16**§§
Formula	$C_{38}H_{41}F_6OsP_3{\cdot}CH_4O$	$C_{38}H_{40}OsP_2$	$C_{76}H_{78}Os_2P_4{\cdot}C_5H_{12}$	$C_{38}H_{42}F_6NOsP_3$	$C_{44}H_{44}OsP_2{\cdot}0.25C_6H_6$
M	926.90	748.89	1567.91	909.87	844.51
Crystal system	Monoclinic	Triclinic	Triclinic	Monoclinic	Triclinic
Space group	$P2_1/n$	$P\bar{1}$	$P\bar{1}$	$P2_1/c$	$P\bar{1}$
a/Å	11.724(1)	11.1341(5)	10.971(2)	11.4255(6)	11.9922(6)
b/Å	17.360(2)	16.7364(8)	17.958(3)	17.3798(8)	17.8922(8)
c/Å	18.500(2)	18.1183(8)	17.855(3)	19.1554(9)	19.8242(9)
α/°		88.689(1)	88.677(4)		114.764(1)
β/°	103.300(2)	88.960(1)	85.690(4)	104.383(1)	90.682(1)
γ/°		70.906(1)	87.946(4)		103.145(1)
V/Å^3	3664	3189	3505	3684	3733
Z	4	4	2	4	4
D_c/g cm^{-3}	1.68_0	1.56_0	1.48_6	1.64_0	1.50_2
μ/cm^{-1}	37	41	38	37	35
Crystal size/mm	0.35 × 0.20 × 0.13	0.18 × 0.18 × 0.10	0.3 × 0.25 × 0.2	0.17 × 0.10 × 0.06	0.24 × 0.20 × 0.08
'T'$_{min/max}$	0.66	0.77	0.71	0.70	0.71
$2\theta_{max}$/°	75	50	76	75	75
N_{tot}	76389	66158	72480	76147	77398
N (R_{int})	19252 (0.054)	11193 (0.063)	36104 (0.041)	19329 (0.044)	38378 (0.049)
N_o	13371	9206	23919	13760	23364
R	0.035	0.042	0.036	0.027	0.038
$R_w(n_w)$	0.035(3)	0.051(5)	0.038(5)	0.024(4)	0.024(0)

Table 4 Comparative electrochemical data for [{Cp(dppe)M}$_2$(μ-C_4)] (M = Fe, Ru, Os)[a]

	Fe (**1**)	Ru (**3**)	Os (**14**)
E^1	−0.68	−0.43	−0.62
E^2	+0.05	+0.22	−0.01
E^3	+0.95	+1.04	+0.82
E^4		+1.51	+1.26[b]
K_c (0/+1/+2)	9.95 × 10^{11}	9.64 × 10^{10}	2.07 × 10^{10}
Ref.	9*a*	11*b*	This work

[a] CH_2Cl_2/0.1 M $[NBu_4]PF_6$, Pt dot working electrode, potentials *vs.* SCE such that $FeCp_2/[FeCp_2]^+$ = 0.46 V. [b] Peak potential of quasi-reversible wave.

Table 5 Ionisation potentials (*IP*, eV) calculated for [{Cp(dHpe)M}$_2$(μ-C_4)]$^{n+}$ (n = 0–4) (M = Fe, Ru, Os)

	Fe (**1-H**)	Ru (**3-H**)	Os (**14-H**)
IP^1	4.789	4.965	4.653
IP^2	8.402	8.386	8.035
IP^3	11.751	11.757	11.361
IP^4	15.438	15.190	14.466
Ref.	15	15	This work

potentials (in solution) and theoretical ionisation potentials (vacuum at 0 K) is observed for each series of complexes [{Cp(dHpe)M}$_2$(μ-C_4)]$^{n+}$ (M = Fe, Ru, Os) with the linear regression coefficient being 0.99 in each case. The only deviation which is noted between experiment and theory concerns the comparison of the first oxidation of the Fe and Os species. The neutral Fe complex is more easily oxidized than the neutral Os analogue (see Table 4), although the reverse is found in the computational work (Table 5). On the other hand, both experiment and theory indicate that the osmium compound becomes the easiest species to oxidise after the second oxidation process, while the iron system is progressively less easily oxidised.

Guided by the electrochemical results, the redox products derived from **14** were examined using IR and UV-Vis-NIR spectroelectrochemical methods as a complement to the data obtained from samples of [**14**]$^{n+}$ salts obtained by chemical oxidation. In CH_2Cl_2 solutions containing 0.1 M $[NBu_4]BF_4$ supporting electrolyte, **14** exhibited a moderately intense ν(C≡C) band at 1970 cm^{-1}, with a shoulder on the higher frequency side. Sequential oxidation of **14** caused a shift in the ν(CC) band to 1870 cm^{-1} ([**14**]$^+$) and 1780 cm^{-1} ([**14**]$^{2+}$) (Fig. 6). The recovery of the spectrum of **14** by stepwise reduction of [**14**]$^{2+}$ in the spectro-electrochemical cell gives confidence in these assignments, as does the excellent agreement of the data with those obtained from samples prepared by chemical oxidation reactions (Table 6). Further oxidation of [**14**]$^{2+}$ gave two further stepwise transformations, with the ν(CC) band shifting initially to 1570 cm^{-1}, and finally to 1960, 1920 cm^{-1}. However, these latter redox products were not chemically robust, with reduction failing to result in the recovery of lower oxidation states of [**14**]$^{n+}$, and we refrain from definitive assignment of these ν(CC) bands to [**14**]$^{3+}$ and [**14**]$^{4+}$. The progression of ν(C≡C) bands observed for the series [**14**]$^{n+}$ may be compared with similar progressions associated with [**1**]$^{n+}$ and [**3**]$^{n+}$ (Table 6).

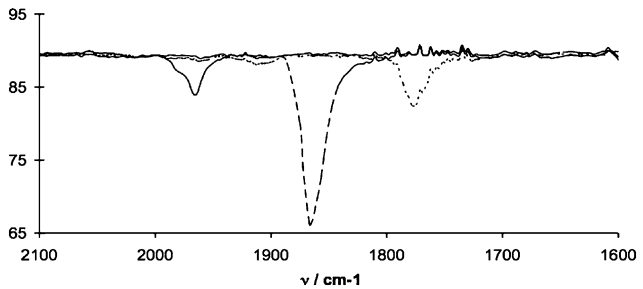

Fig. 6 The spectro-electrochemically generated IR [ν(C≡C)] spectra of **14** (——), [**14**]$^+$ (---) and [**14**]$^{2+}$ (· · ·).

Table 6 IR spectroscopic data (ν(CC)/cm^{-1}) from the complexes [{M(dppe)Cp*}$_2$(μ-C$_4$)]$^{n+}$

	M = Fe[a]	M = Ru[b]	M = Os[b]
$n = 0$	1880, 1955	1963, 1977sh	1965, 1975sh
$n = 1$	1880, 1973	1860	1860
$n = 2$	1950, 2160	1770	1781

[a] CH_2Cl_2 solution. [b] Nujol mull.

The data in Table 6 clearly demonstrate the remarkable similarity of the ruthenium ([**3**]$^{n+}$) and osmium [**14**]$^{n+}$ complexes, and the equally remarkable distinction from the iron analogue [**1**]$^{n+}$. The IR data from [**1**]$^{n+}$ have been interpreted in terms of largely metal-centred frontier orbitals on the basis of corroborative Mössbauer spectroscopy and computational analysis. In contrast, the more diffuse d-orbitals on the ruthenium lead to more extensively delocalised frontier orbitals with considerable metal and carbon bridging ligand character. Consequently, oxidation of **3** leads to a decrease in the C≡C bonding character and a gradual progression from a buta-1,3-diynediyl structure (Scheme 2, **G**) to more cumulated structures (Scheme 2, **H**) and, ultimately, to an ethynediyl-bridged dicarbyne (Scheme 2, **I**) as the formal electron count is reduced.[2,11,27] The virtually identical IR data obtained from [**14**]$^{n+}$ and [**3**]$^{n+}$ indicate that the carbon ligands in both series are comparable in each oxidation state, as found for the optimized geometries (see above).

The UV-Vis-NIR spectrum of **14** was relatively featureless, with only the low energy tail of high energy UV bands apparent in the visible region, and responsible for the colour of this complex. The monocationic complex [**14**]$^+$ exhibited more distinct features at 27 800 cm^{-1} (ε 11 500 M^{-1} cm^{-1}) and a broad series of overlapping transitions between 19000–8000 cm^{-1} (Fig. 7). The electronic spectrum of the dicationic complex [**14**]$^{2+}$ was dominated by intense bands at 34 000 cm^{-1} (ε 24 000 M^{-1} cm^{-1}), 28 000 cm^{-1} (ε 16 000 M^{-1} cm^{-1}) and 17 100 cm^{-1} (ε 20 000 M^{-1} cm^{-1}). A shoulder at 19 350 cm^{-1} (ε 7100 M^{-1} cm^{-1}) was also evident, as was a lower intensity band near 13 400 cm^{-1} (ε 3200 M^{-1} cm^{-1}). These general features are very similar to those observed in the ruthenium series [**2**]$^{n+}$ and [**3**]$^{n+}$ (n = 0–3).[11]

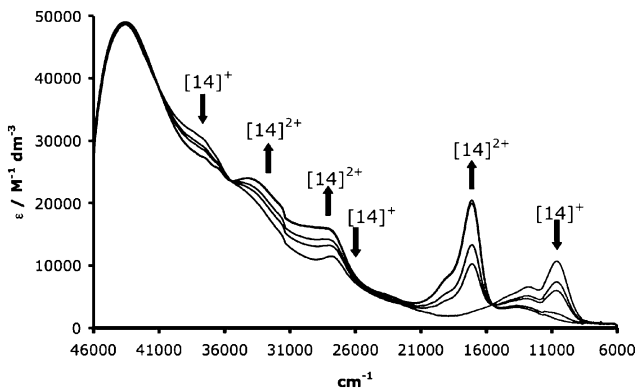

Fig. 7 The spectro-electrochemical conversion of [**14**]$^+$ to [**14**]$^{2+}$ (CH_2Cl_2/0.1 M [NBu$_4$]BF$_4$).

The analysis of NIR bands exhibited by radical cations of general form {[ML$_x$](μ-X)[M′L$_x$]}$^+$, where X is some conjugated bridge, has been a topic of considerable interest for many years, with the interpretations usually being derived from the classical discussions of mixed-valence complexes based on a two-state model of weakly interacting metal centres.[28] However, in systems where the bridge orbitals are significantly involved in the semi-occupied molecular orbitals, the two-state model breaks down.[29] The frontier orbitals of poly-ynediyl complexes are, in the simplest terms, derived from linear combinations of the metal d and C$_n$ π type orbitals.[27] In the case of complexes derived from d^6 metal fragments the highest lying orbitals have been thoroughly described, being of π-symmetry, delocalised over the MC$_4$M chain with nodal planes between M–C and ≡C–C≡ fragments. The relative contributions from metal and carbon-based orbitals to the HOMO (and orthogonal HOMO − 1) is determined by both the nature of the metal and the length of the polycarbon fragment,[2,9,11,12,15] Indeed, the HOMOs are similar in character for [**14-H**] and its neutral Ru analogue, with metallic and carbon chain character percentages of 24/59 and 26/62 for the HOMO, and 22/68 and 21/69 for HOMO − 1, respectively. The HOMOs of the iron species show a much stronger metallic character percentage: 41 (Fe$_2$)/46 (C$_4$ chain) for the HOMO and 36 (Fe$_2$)/52 (C$_4$ chain) for the HOMO − 1. Consequently different behaviour can be found between examples containing, for example, iron on the one hand[9] and ruthenium, osmium, and rhenium on the other.[7,11] Oxidation results in depopulation of these high-lying orbitals, which has been confirmed by the available vibrational and structural data, as well as by computational investigations.[15] Consequently the frontier orbitals in cations such as [{M(L)$_2$Cp}$_2$(μ-C$_n$)]$^+$ are rather similar to the HOMOs of the analogous compounds [{M(L)$_2$Cp}$_2$(μ-C$_n$)].

Very recently, TD-DFT calculations on MC$_2$M systems have indicated that the NIR bands in diruthenium ethynediyl systems [{Ru(dHpe)Cp}$_2$(μ-C$_2$)]$^+$ are derived from transitions between orbitals which are rather heavily metal/phosphine/Cp in character and the semi-occupied (or more precisely, β-LUSO) orbital which has considerable [M(d)/C$_n$(π)]* character.[14] These bands can therefore be approximately described as being metal-to-(metal–ligand) charge transfer in character. The calculated electronic excitations for [**14-H**]$^+$ in its most favoured orientation (metallic fragments in *trans* position) contain only one strong excitation in the NIR region at 15 324 cm^{-1} (oscillator strength = 0.28). It is mainly a transition between the β-SOMO − 1 and the β-LUSO, involving a metal-to-(metal–ligand) charge transfer process. Several absorption bands are experimentally observed in this NIR region. They are most probably due to the superposition of the spectra of the different conformations adopted in solution. The next electronic excitations with a non-negligible oscillator strength are calculated at 27 818 and 28 367 cm^{-1}, in agreement with the experimental measurements (27 800 cm^{-1}). They involve charge transfer, mainly metal–carbon chain-to-ligand (phosphine π* orbitals) in character. The most significant feature in the experimental spectra of [**14**]$^{2+}$ is the intense absorption near 17 240 cm^{-1}, which has a rather similar profile to the NIR band observed in [**14**]$^+$ and also to the visible absorption bands observed in [{Ru(dppe)Cp}$_2$(μ-C$_2$)]$^{2+}$, [**2**]$^{2+}$ and [**3**]$^{2+}$. The visible band observed in [**14**]$^{2+}$ can therefore be attributed to transitions between occupied metal-centred orbitals and an unoccupied [M(d)/C$_4$(π)M(d)]* orbital, noting that the semi-occupied orbital in [**14**]$^+$ (LUSO) is the LUMO in the (singlet) [**14**]$^{2+}$.

Conclusion

The synthesis and characterisation of **14** completes the first isoleptic series of butadiynediyl complexes derived from members of the same metal triad. The osmium complex **14** is readily oxidised at modest potentials to afford a range of mono-, di-, tri- and tetra-cationic derivatives, the spectroscopic properties of which are generally similar to those described for the ruthenium analogues. The lighter first-row transition metal butadiynediyl complex derived from iron exhibits largely metal-centred redox events, whilst the heavier second- and third-row systems based on ruthenium and osmium feature more carbon character in the redox-active orbitals, as evidenced by the significant shifts in ν(CC) frequencies which accompany oxidation. When these observations are taken together with the other systematic studies of poly-ynediyl complexes [{M(L)$_2$Cp′}$_2$(μ-C$_n$)] that have been reported, it can be concluded that metal contributions to the frontier orbitals are most pronounced in systems containing the lighter metals and for shorter length polycarbon chains. Heavier metals and longer carbon chains promote more carbon-character in the frontier orbitals of these bimetallic derivatives of carbyne.

Experimental

General

All reactions were carried out under high purity dry nitrogen or argon using standard Schlenk techniques, although normally no special precautions to exclude air were taken during subsequent work-up. Common solvents were dried, distilled under argon and degassed before use. Separations were carried out by preparative thin-layer chromatography on glass plates (20 × 20 cm^2) coated with silica gel (Merck, 0.5 mm thick).

Instruments

IR spectra were obtained on a Bruker IFS28 FT-IR spectrometer. Spectra in CH_2Cl_2 were obtained using a 0.5 mm path-length solution cell with NaCl windows. Nujol mull spectra were obtained from samples mounted between NaCl discs. NMR spectra were recorded using Varian 2000 [199.98 MHz (^{1}H), 50.29 MHz (^{13}C)], ACP-300 [300.145 MHz (^{1}H), 75.47 MHz (^{13}C), 121.105 MHz (^{31}P)] or Varian Inova 600 [599.957 MHz (^{1}H), 150.87 MHz (^{13}C), 242.21 MHz (^{31}P)] instruments. Unless otherwise stated, samples were dissolved in $CDCl_3$ contained in 5 mm sample tubes. Chemical shifts are given in ppm relative to internal tetramethylsilane for ^{1}H and ^{13}C NMR spectra and external H_3PO_4 for ^{31}P NMR spectra. UV-Vis spectra were recorded on a Varian Cary 5 UV-Vis/NIR spectrometer. Electrospray mass-spectrometry (ES-MS) was carried out at the University of Waikato, Hamilton, New Zealand. Spectra were obtained from samples dissolved in MeOH unless otherwise indicated. Solutions were injected into a Varian Platform II spectrometer *via* a 10 ml injection loop. Nitrogen was used as the drying and nebulising gas. Chemical aids to ionisation were used.[30]

Electrochemical samples (10^{-3} M) were dissolved in CH_2Cl_2 containing 5 × 10^{-1} M [NBu_4]BF_4 as the supporting electrolyte. Cyclic voltammograms were recorded using a Princeton Applied Research model 263 apparatus, with a saturated calomel electrode, with ferrocene as internal calibrant ($FeCp_2/[FeCp_2]^+ = 0.46$ V).

Infrared spectroelectrochemical experiments were conducted with a demountable OTTLE cell fitted with CaF_2 windows.[31] The solutions were 10^{-1} M in the supporting electrolyte ([NBu_4]BF_4) and 5 × 10^{-3} M in the analyte. The working electrode potential of the spectro-electrochemical cell was controlled with a home-built potentiostat. The IR spectra were recorded with Nicolet Avatar FT-IR spectrometers (35 scans, 1–2 cm^{-1} spectral resolution). UV-Vis-NIR spectro-electrochemical experiments were carried out in the same cell using solutions in CH_2Cl_2 containing 10^{-1} M [NBu_4]BF_4 as supporting electrolyte on a Varian Cary 5 spectrophotometer. Analyte concentration was 6.7 × 10^{-4} M. All solvents were deoxygenated with dry nitrogen prior to use, and the cell was filled under a nitrogen atmosphere.

Elemental analyses were performed by Chemical and Micro-Analytical Services (CMAS), Belmont, Victoria.

Reagents

The compounds HCp*,[32] $Me_3SiC{\equiv}CH$,[33] $Me_3SiC{\equiv}CC{\equiv}CSiMe_3$,[34] and [$FeCp_2$]$PF_6$[35] were prepared by the cited methods. All other reagents were used as received without further purification.

Syntheses

PRECAUTIONARY WARNING: OsO_4 is extremely toxic. The yellow solid melts at 31 °C and has an appreciable vapour pressure even at room temperature. The compound is often liberated when solutions of osmium compounds are treated with oxidising agents. Ample precautions to protect eyes, nose and mouth are essential.

Preparation of [{Os(μ-Br)BrCp*}$_2$]. An ampoule of OsO_4 (1.0 g, 3.93 mmol) was broken and immediately dropped into a flask containing 48% HBr (37 mL). The resulting deep red solution was heated at reflux point for 2 h in air. The solution was decanted into another flask and the original flask containing the broken glass was rinsed with an additional 10 mL of HBr. Water and excess HBr were removed from the combined solutions under vacuum at 50 °C, leaving a dark red-brown residue which was dried under high vacuum for 16 h, to give H_2OsBr_6 as a red-brown solid (2.64 g, 100%). A suspension of H_2OsBr_6 (2.62 g, 3.90 mmol) and Cp*H (796 mg, 5.85 mmol, 1.5 eq.) in ethanol (50 mL) was de-oxygenated by bubbling nitrogen through the suspension for 15 min. The de-oxygenated suspension was heated at reflux point for 40 min and allowed to cool for 5 min. The resultant dark brown solution was decanted using Schlenk techniques, with strict exclusion of oxygen, to leave [{Os(μ-Br)BrCp*}$_2$] as a black-brown precipitate which was used immediately in the next step without further purification. ^{1}H NMR ($CDCl_3$): δ_H 2.40 (s, 15H, Cp*). ^{13}C NMR ($CDCl_3$): δ_C 108.42 (s, Cp*), 13.65 (s, Cp*).

[OsBr(cod)Cp*] (9). 1,5-Cyclooctadiene (2.52 mL, 20.6 mmol) and ethanol (40 mL) were added to a Schlenk flask containing [{Os(μ-Br)BrCp*}$_2$] (prepared as above) and the suspension was de-oxygenated (as above). The suspension was heated at reflux point for 90 min during which time the orange colour of the solution darkened. Solvent was removed under vacuum and the dark brown residue was extracted with boiling diethyl ether (4 × 30 mL). The combined orange extracts were filtered and solvent was removed under vacuum to give [OsBr(cod)Cp*] (**9**) as a dark orange solid (1.07 g, 54%). ^{1}H NMR ($CDCl_3$): δ 1.68 (s, 15H,

Cp*), 1.71 (m, 2H, CH_2), 1.95 (m, 2H, CH_2), 2.19 (m, 2H, CH_2), 2.62 (m, 2H, CH_2), 3.62 (m, 1H, CH), 4.07 (m, 1H, CH). ^{13}C NMR ($CDCl_3$): δ 94.01 (s, Cp*), 69.3 (s, CH), 68.1 (s, CH), 33.2 (s, CH_2), 9.82 (s, Cp*).

[OsBr(dppe)Cp*] (10). A suspension of [OsBr(cod)Cp*] (930 mg, 1.81 mmol) and dppe (722 mg, 1.81 mmol) in heptane (40 mL) was heated at reflux point under nitrogen for 16 h. After cooling, the resulting precipitate was collected by vacuum filtration and washed with heptane (3 × 10 ml) to give [OsBr(dppe)Cp*] (**10**) as a pale orange powder (1.18 g, 81%). Anal. calcd ($C_{36}H_{39}P_2OsBr$): C, 53.80; H, 4.89; *M*, 803. Found: C, 53.51; H, 4.94%. IR (Nujol): 1092 s, 1023 m, 786 m, 741 s, 700 vs, 665 s cm^{-1}. ^{1}H NMR (C_6D_6): δ 1.61 (s, 15H, Cp*), 2.09, 2.62 (2 × m, 2 × H, PCH_2), 6.97–7.92 (m, 20H, Ph). ^{13}C NMR (C_6D_6): δ 9.51 (s, Cp*), 30.77 (m, PCH_2), 85.12 [t, *J*(CP) = 3 Hz, Cp*], 127.75–140.86 (m, Ph). ^{31}P NMR (C_6D_6): δ 43.0 (s). ES-MS (positive ion mode, *m*/*z*): 804, M^+; 725, $[Os(dppe)Cp^*]^+$.

[Os(=C=CH$_2$)(dppe)Cp*]PF$_6$ ([11]PF$_6$). $HC{\equiv}CSiMe_3$ (55 mg, 0.558 mmol, 5 mol eq.) was added to a suspension of [OsBr(dppe)Cp*] (100 mg, 0.112 mmol) and $[NH_4]PF_6$ (36.3 mg, 0.223 mmol, 2 mol eq.) in CH_2Cl_2 (15 mL), and the mixture was stirred at 45 °C for 72 h in a sealed Schlenk flask. The resulting suspension was filtered to remove precipitated NH_4Br and added dropwise to rapidly stirred diethyl ether to give $[Os(=C=CH_2)(dppe)Cp^*]PF_6$ ([**11**]PF$_6$) (89 mg, 90%) as a pale yellow powder that was collected by vacuum filtration and dried under high vacuum. An analytical sample was obtained from methanol and obtained as the methanol solvate. Anal. calcd ($C_{38}H_{41}F_6P_3Os{\cdot}MeOH$): C, 50.54; H, 4.89; *M* (cation), 751. Found: C, 50.31; H, 4.79%. IR (Nujol): *ν*(C=C) 1633, *ν*(PF) 836 cm^{-1}. ^{1}H NMR ($CDCl_3$): δ 0.66 (s, 2H, $=CH_2$), 1.73 [t, *J*(HP) 1 Hz, 15H, Cp*], 2.70–2.94 (m, 4H, PCH_2), 7.15–7.65 (m, 20H, Ph). ^{13}C NMR ($CDCl_3$): δ 9.72 (s, Cp*), 30.58–31.23 (m, PCH_2), 92.17 (s, Cp*), 100.64 (m, C_β), 128.86–133.91 (m, Ph), 305.27 [t, *J*(CP) 10 Hz, C_α]. ^{31}P NMR ($CDCl_3$): δ 40.8 (s, PPh), −143.7 [septet, *J*(PF) = 711 Hz, PF_6]. ES-MS (positive ion mode, *m*/*z*): 751, $[M - PF_6]^+$.

[Os(C≡CH)(dppe)Cp*] (12).

Method (a). Thoroughly de-oxygenated THF (15 mL) was transferred *via* cannula to a Schlenk flask containing $[Os(=C=CH_2)(dppe)Cp^*]PF_6$ **7** (88 mg, 0.098 mmol) and KOBu^t (11.4 mg, 0.098 mmol, 1 mol eq.) in an atmosphere of argon, and the resulting yellow solution was stirred at room temperature for 30 min. The solvent was removed under vacuum and the resultant solid was extracted with benzene and filtered to remove residual KPF_6. The solvent was removed under vacuum to give [Os(C≡CH)(dppe)Cp*] (**12**) as a yellow solid that was dried under high vacuum (44 mg, 59%).

Method (b). A suspension of [OsBr(dppe)Cp*] (200 mg, 0.248 mmol) and $HC{\equiv}CSiMe_3$ (245 mg, 2.48 mmol, 10 eq.) in EtOH (30 mL) was stirred in a sealed Schlenk flask at 45 °C for 5 d under nitrogen. The resulting orange solution was cooled in ice and a freshly prepared NaOEt solution (25 mg Na in EtOH; 5 mL) was added dropwise with stirring. An immediate colour change from orange to pale yellow occurred and a pale yellow precipitate separated. This was collected by vacuum filtration, washed with ice-cold EtOH (3 × 5 mL) and dried under high vacuum to give [Os(C≡CH)(dppe)Cp*] (**12**) as a pale yellow powder (101 mg, 61%). Anal. calcd ($C_{38}H_{40}P_2Os$): C, 60.95; H, 5.38; *M*, 750. Found: C, 60.81; H, 5.39%. IR (Nujol): *ν*(≡CH) 3274, *ν*(C≡C) 1929 cm^{-1}. ^{1}H NMR (C_6D_6): δ 1.73 (s, 15H, Cp*), 2.10 (s, 1H, C≡CH), 2.03, 2.69 (2 × m, 2 × 2H, PCH_2), 7.03–7.95 (m, 20H, Ph). ^{13}C NMR (C_6D_6): δ 10.04 (s, Cp*), 31.16 (m, PCH_2), 88.79 [t, *J* (CP) 2.7 Hz, Cp*], 89.88 (s, C_β), 92.91 [t, *J*(CP) 17 Hz, C_α], 127.02–139.37 (m, Ph). ^{31}P NMR (C_6D_6): δ 43.6 (s). ES-MS (positive ion mode, *m*/*z*): 751, $[M + H]^+$.

[{Os(dppe)Cp*}$_2${μ-(=C=CH–CH=C=)}](PF$_6$)$_2$ ([13](PF$_6$)$_2$). Thoroughly de-oxygenated CH_2Cl_2 (20 mL) was cooled to −78 °C and transferred *via* cannula to a Schlenk flask cooled to −78 °C and containing [Os(C≡CH)(dppe)Cp*] **12** (150 mg, 0.20 mmol) and $[FeCp_2]PF_6$ (63 mg, 0.19 mmol, 0.95 eq.) under argon. The solution was stirred for 3 h at −78 °C and then allowed to warm to r.t. over 12 h. The solution was then filtered into rapidly stirred hexane to give a gray solid which was collected by vacuum filtration, washed with hexane (2 × 5 mL) and dried under high vacuum to give $[\{Os(dppe)Cp^*\}_2\{\mu\text{-}(=C=CHCH=C=)\}](PF_6)_2$ ([**13**](PF$_6$)$_2$) as a pale gray solid (126 mg, 74%). IR (Nujol): *ν*(C=C) 1611, *ν*(PF) 841 cm^{-1}. ^{1}H NMR ($CDCl_3$): δ 1.00 (s, 2H, =CH), 1.73 (s, 30H, Cp*), 2.60–2.72 (m, 8H, PCH_2), 7.00–7.56 (m, 40H, Ph). ^{13}C NMR ($CDCl_3$): δ 9.46 (s, Cp*), 30.21–31.87 (m, PCH_2), 88.21 (s, Cp*), 100.37 (s, C_β), 128.62–134.32 (m, Ph), 309.69 (s, C_α). ^{31}P NMR ($CDCl_3$): δ 39.5 (s, PPh_3), −143.7 [septet, *J*(PF) = 711 Hz, PF_6]. ES-MS (positive ion mode, *m*/*z*): 749, M^{2+} (calcd M^{2+}, 749).

[{Os(dppe)Cp*}$_2$(μ-C≡CC≡C)] (14). Thoroughly de-oxygenated THF (20 mL) was transferred *via* cannula to a Schlenk flask containing $[\{Os(dppe)Cp^*\}_2\{\mu\text{-}(=C=CHCH=C=)\}](PF_6)_2$ (**13**) (125 mg, 0.07 mmol) and KOBu^t (15.5 mg, 0.139 mmol, 2 eq.) under argon, and the solution was stirred at r.t. for 30 min. Solvent was removed under vacuum and the crude solid was extracted with hexane (3 × 5 mL) to give a bright orange solution which was filtered to remove residual KPF_6. Solvent was removed to give $[\{Os(dppe)Cp^*\}_2(\mu\text{-}C{\equiv}CC{\equiv}C)]$ (**14**) as a bright orange powder (65 mg, 66%). Anal. calcd ($C_{76}H_{78}P_4Os_2$): C, 61.03; H, 5.26; *M*, 1497. Found: C, 61.15; H, 5.34%. IR (Nujol): *ν*(C≡C) 1965 s cm^{-1}. ^{1}H NMR (C_6D_6): δ 1.75 (s, 30H, Cp*), 2.03, 2.64 (2 × m, 2 × 4H, PCH_2), 7.06–7.99 (m, 40H, Ph). ^{13}C NMR (C_6D_6): δ 10.08 (s, Cp*), 31.39 (m, PCH_2), 71.32 [t, *J*(CP) 19 Hz, C_α], 88.68 (s, Cp*), 95.46 (s, C_β), 127.16–139.99 (m, Ph). ^{13}P NMR (C_6D_6): δ 43.6 (s). ES-MS (positive ion mode, *m*/*z*): 1496, M^+.

[{Os(dppe)Cp*}$_2$(μ-C$_4$)]PF$_6$ ([14]PF$_6$). $[FeCp_2]PF_6$ (5.4 mg, 0.016 mmol) was added to a solution of $[\{Os(dppe)Cp^*\}_2(\mu\text{-}C{\equiv}CC{\equiv}C)]$ (26 mg, 0.017 mmol) in CH_2Cl_2 (10 ml). The colour changed immediately from orange to green. After stirring for 30 min, the volume was reduced to 2 ml and hexane (25 ml) was added dropwise to give green $[\{Os(dppe)Cp^*\}_2(\mu\text{-}C_4)]PF_6$ ([**14**]PF$_6$) (20 mg, 72%). IR (Nujol, cm^{-1}): *ν*(CC) 1860 w, *ν*(PF) 839 s. ^{1}H NMR (d_6-acetone): δ 7.36–8.22 (br m, 40H, Ph), 10.68 (br, 8H, CH_2), 12.16 (br, 30H, Cp*). ES-MS (positive ion, MeOH, *m*/*z*): 1496, M^+; 725, $[Os(dppe)Cp^*]^+$.

[{Os(dppe)Cp*}$_2$(μ-C$_4$)](PF$_6$)$_2$ ([14](PF$_6$)$_2$). A similar reaction to the above, using $[\{Os(dppe)Cp^*\}_2(\mu\text{-}C{\equiv}CC{\equiv}C)]$ (10 mg, 0.007 mmol) and $[FeCp_2]PF_6$ (4.3 mg, 0.013 mmol) in CH_2Cl_2 (10 ml), resulted in colour changes from orange to green to deep blue. After stirring for 30 min, reduction in volume to 2 ml and addition of hexane (25 ml) resulted in precipitation of

dark blue [{Os(dppe)Cp*}$_2$(μ-C_4)](PF$_6$)$_2$ ([**14**](PF$_6$)$_2$) (8 mg, 67%). Anal. calcd ($C_{76}H_{70}F_{12}Os_2P_6$): C, 51.12; H, 4.40; *M* (cation), 1496. Found: C, 51.09; H, 4.31%. IR (Nujol, cm^{-1}): *ν*(CC) 1781 w, *ν*(PF) 836 s. ^{1}H NMR (d_6-acetone): *δ* 2.13 (br, 30H, Cp*), 3.19–3.31, 3.58–3.69 (2 × m, 2 × 4H, CH_2), 6.99–7.80 (m, 40H, Ph). ^{31}P NMR (d_6-acetone): *δ* 81.0 (dppe), −143.0 (sept, PF_6). ES-MS (positive ion, MeOH, *m*/*z*): 748, M^{2+}; 725, [Os(dppe)Cp*]$^+$.

[Os(NCMe)(dppe)Cp*]PF$_6$ ([15]PF$_6$). A suspension of OsBr(dppe)Cp* (100 mg, 0.124 mmol) and [NH_4]PF_6 (20.5 mg, 0.124 mmol) in MeCN (15 mL) was heated at reflux point for 20 h. After this time the reaction mixture consisted of solid NH_4Br under a pale yellow solution. Filtration and removal of solvent under vacuum was followed by dissolving the yellow residue in CH_2Cl_2 (5 mL) and adding the solution dropwise to rapidly stirred diethyl ether. The off-white precipitate was collected by vacuum filtration, washed with diethyl ether (3 × 5 mL) and dried under high vacuum to give pure [Os(NCMe)(dppe)Cp*]PF_6 ([**15**]PF_6) (84 mg, 74%). Anal. calcd ($C_{38}H_{42}P_3F_6OsN$): C, 50.16; H, 4.65; *M* (cation), 766. Found: C, 49.95; H, 4.97%. IR (Nujol): *ν*(C≡N) 2264, *ν*(PF) 838 cm^{-1}. ^{1}H NMR ($CDCl_3$): *δ* 1.51 (s, 15H, Cp*), 1.80 (s, 3H, Me), 2.35–2.56 (m, 4H, PCH_2), 7.21–7.55 (m, 20H, Ph). ^{13}C NMR ($CDCl_3$): *δ* 3.49 (s, CH_3), 9.58 (s, Cp*), 30.68 (m, PCH_2), 89.34 [t, *J*(CP) = 3 Hz, Cp*], 119.62 (s, C≡N), 128.72–135.25 (m, Ph). ^{31}P NMR ($CDCl_3$): *δ* 43.3 (s, PCH_2), −143.7 [septet, ^{1}*J*(PF) = 711 Hz, PF_6]. ES-MS (positive ion mode, *m*/*z*): 766, [M − PF_6]$^+$.

[Os(C≡CPh)(dppe)Cp*] (16). A suspension of [OsBr(dppe)Cp*] (100 mg, 0.124 mmol) and HC≡CPh (32.3 mg, 0.335 mmol) in EtOH (10 mL) was heated at reflux point for 17 h. The resulting orange solution was cooled on ice and a freshly prepared NaOEt solution (Na, 25 mg, in ethanol, 5 mL) was added dropwise with stirring. An immediate colour change from orange to pale yellow was observed and a pale yellow precipitate separated. This was collected by vacuum filtration, washed with ice-cold ethanol (3 × 5 mL) and dried under high vacuum to give [Os(C≡CPh)(dppe)Cp*] (**16**) as a pale yellow powder (67.2 mg, 63%). Concentration of the filtrate gave a further 21.2 mg of product (total yield, 83%). Anal. calcd ($C_{44}H_{44}P_2Os$): C, 64.06; H, 5.37. Found: C, 63.94; H, 5.34%. IR (Nujol): *ν*(C≡C) 2085 cm^{-1}. ^{1}H NMR ($CDCl_3$): *δ* 1.68 (s, 15H, Cp*), 2.12, 2.61 (2 × m, 2 × H, PCH_2), 6.72–8.14 (m, 25H, Ph). ^{13}C NMR ($CDCl_3$): *δ* 10.00 (s, C_5Me_5), 31.38 (m, PCH_2), 89.19 (s, C_5Me_5), 97.04 (s, $C_β$), 105.99 [t, *J*(CP) 19.6 Hz, C_a], 127.07–139.92 (m, Ph). ^{31}P NMR ($CDCl_3$): *δ* 43.7 (s).

Structure determinations

Full spheres of diffraction data were measured at *ca.* 153 K using a Bruker AXS CCD area-detector instrument. N_{tot} reflections were merged to *N* unique (R_{int} cited) after "empirical"/multiscan absorption correction (proprietary software), N_o with $F > 4\sigma(F)$ being used in the full matrix least squares refinements. All data were measured using monochromatic Mo-Kα radiation, $\lambda = 0.71073$ Å. Anisotropic displacement parameter forms were refined for the non-hydrogen atoms, (x, y, z, U_{iso})$_H$ being included, constrained at estimates. Conventional residuals *R*, R_w on |*F*| are quoted [weights: $(\sigma^2(F) + 0.000n_wF^2)^{-1}$]. Neutral atom complex scattering factors were used; computation used the XTAL 3.7 program system.[36] Pertinent results are given in the figures (which show non-hydrogen atoms with 50% probability amplitude displacement ellipsoids and hydrogen atoms with arbitrary radii of 0.1 Å) and in Tables 1–3.

Density functional calculations

DFT calculations were performed with the amsterdam density functional package (ADF 2005)[37] on models [**14-H**]$^{n+}$ (phenyl groups were replaced by hydrogen atoms), $n = 0, 1, 2, 3, 4$. The singlet and triplet states were considered for [**14-H**]$^{2+}$. The geometries were fully optimized without constraints (C_1 symmetry). Electron correlation was treated within the local density approximation (LDA) in the Vosko–Wilk–Nusair parametrization.[38] The non-local corrections of Becke and Perdew were added to the exchange and correlation energies, respectively.[39] The analytical gradient method implemented by Verluis and Ziegler was used.[40] The standard ADF TZP basis set was used, *i.e.*, triple-ξ STO basis set for the valence core augmented with a 3d polarisation function for C, P, and a 6p polarisation function for Os. Orbitals up to 1s, 2p, and 4f were kept frozen for C, P, and Os, respectively. Relativistic corrections were added using the ZORA (zeroth order regular approximation) scalar Hamiltonian.[41] The excitation energies and oscillator strengths were calculated following the procedure described by van Gisbergen and cowokers.[42] The ionisation potentials were computed adiabatically.

Acknowledgements

We thank the ARC for support of this work and Johnson Matthey plc, Reading, for generous loans of $RuCl_3 \cdot nH_2O$ and potassium osmate. These studies were facilitated by travel grants (ARC, Australia; the Royal Society of Chemistry, UK; the CNRS, France).

References

1 (*a*) F. Paul and C. Lapinte, in *Unusual Structures and Physical Properties in Organometallic Chemistry*, ed. M. Gielen, R. Willem and B. Wrackmeyer, Wiley, New York, 2002, pp. 220–291; (*b*) J. M. Tour, *Acc. Chem. Res.*, 2000, **33**, 791; (*c*) F. Paul and C. Lapinte, *Coord. Chem. Rev.*, 1998, **178–180**, 431; (*d*) M. D. Ward, *Chem. Soc. Rev.*, 1995, **24**, 121; (*e*) U. H. F. Bunz, *Angew. Chem., Int. Ed. Engl.*, 1994, **33**, 1073; (*f*) H. Lang, *Angew. Chem., Int. Ed. Engl.*, 1994, **33**, 547; F. Diederich and Y. Rubin, *Angew. Chem., Int. Ed. Engl.*, 1992, **31**, 1101.
2 M. I. Bruce and P. J. Low, *Adv. Organomet. Chem.*, 2004, **50**, 179.
3 (*a*) L. de Quadras, F. Hampel and J. A. Gladysz, *Dalton Trans.*, 2006, 2929; (*b*) T. B. Peters, J. C. Bohling, A. M. Arif and J. A. Gladysz, *Organometallics*, 1999, **18**, 3261; (*c*) Q. Zheng and J. A. Gladysz, *J. Am. Chem. Soc.*, 2005, **127**, 10508; (*d*) G. R. Owen, J. Stahl, F. Hampel and J. A. Gladysz, *Organometallics*, 2004, **23**, 5889; (*e*) G. R. Owen, F. Hampel and J. A. Gladysz, *Organometallics*, 2004, **23**, 5893; (*f*) Q. Zheng, F. Hampel and J. A. Gladysz, *Organometallics*, 2004, **23**, 5896; (*g*) W. Mohr, J. Stahl, F. Hampel and J. A. Gladysz, *Inorg. Chem.*, 2001, **40**, 3263.
4 (*a*) S. Kheradmandan, K. Heinze, H. W. Schmalle and H. Berke, *Angew. Chem., Int. Ed.*, 1999, **38**, 2270; (*b*) F. J. Fernandez, O. Blacque, M. Alfonso and H. Berke, *Chem. Commun.*, 2001, 1266; (*c*) F. J. Fernandez, K. Venkatesan, O. Blacque, M. Alfonso, H. W. Schmalle and H. Berke, *Chem.–Eur. J.*, 2003, **9**, 6192.
5 S. Kheradmandan, K. Venkatesan, O. Blacque, H. W. Schmalle and H. Berke, *Chem.–Eur. J.*, 2004, **10**, 4872.
6 K. Venkatesan, T. Fox, H. W. Schmalle and H. Berke, *Organometallics*, 2005, **24**, 2834.
7 (*a*) M. Brady, W. Weng, Y. Zhou, J. W. Seyler, A. J. Amoroso, A. M. Arif, M. Böhme, G. Frenking and J. A. Gladysz, *J. Am. Chem. Soc.*,

1997, **119**, 775; (*b*) R. Dembinski, T. Lis, S. Szafert, C. L. Mayne, T. Bartik and J. A. Gladysz, *J. Organomet. Chem.*, 1999, **578**, 229; (*c*) R. Dembinski, T. Bartik, B. Bartik, M. Jaeger and J. A. Gladysz, *J. Am. Chem. Soc.*, 2000, **122**, 810.
8 M. Akita, M. C. Chung, A. Sakurai, S. Sugimoto, M. Terada, M. Tanaka and Y. Moro-oka, *Organometallics*, 1997, **16**, 4882.
9 (*a*) N. Le Narvor, L. Toupet and C. Lapinte, *J. Am. Chem. Soc.*, 1995, **117**, 7129; (*b*) F. Coat and C. Lapinte, *Organometallics*, 1996, **15**, 477; (*c*) F. Coat, M.-A. Guillevic, L. Toupet and C. Lapinte, *Organometallics*, 1997, **16**, 5988; (*d*) N. Le Narvor and C. Lapinte, *C. R. Acad. Sci., Ser. IIc: Chim.*, 1998, **1**, 745.
10 M. Guillemot, L. Toupet and C. Lapinte, *Organometallics*, 1998, **17**, 1928.
11 (*a*) M. I. Bruce, P. J. Low, K. Costuas, J.-F. Halet, S. P. Best and G. A. Heath, *J. Am. Chem. Soc.*, 2000, **122**, 1949; (*b*) M. I. Bruce, B. G. Ellis, P. J. Low, B. W. Skelton and A. H. White, *Organometallics*, 2003, **22**, 3184; (*c*) M. I. Bruce, B. C. Hall, B. D. Kelly, P. J. Low, B. W. Skelton and A. H. White, *J. Chem. Soc., Dalton Trans.*, 1999, 3719.
12 (*a*) F. Zhuravlev and J. A. Gladysz, *Chem.–Eur. J.*, 2004, **10**, 6510; (*b*) H. J. Jiao, K. Costuas, J. A. Gladysz, J.-F. Halet, M. Guillemot, L. Toupet, F. Paul and C. Lapinte, *J. Am. Chem. Soc.*, 2003, **125**, 9511; (*c*) C. Herrmann, J. Neugebauer, J. A. Gladysz and M. Reiher, *Inorg. Chem.*, 2005, **44**, 6174.
13 Z. X. Cao and Q. Zhang, *Chem.–Eur. J.*, 2004, **10**, 1920.
14 M. I. Bruce, K. Costuas, B. G. Ellis, J.-F. Halet, P. J. Low, B. Moubaraki, K. S. Murray, N. Ouddaï, G. J. Perkins, B. W. Skelton and A. H. White, *Organometallics*, 2007, **26**, 3735.
15 M. I. Bruce, K. Costuas, T. Davin, B. G. Ellis, J.-F. Halet, C. Lapinte, P. J. Low, M. E. Smith, B. W. Skelton, L. Toupet and A. H. White, *Organometallics*, 2005, **24**, 3864.
16 F. P. Dwyer and J. W. Hogarth, *Inorg. Synth.*, 1957, **5**, 204.
17 (*a*) C. L. Gross, S. R. Wilson and G. S. Girolami, *J. Am. Chem. Soc.*, 1994, **116**, 10294; (*b*) C. L. Gross and G. S. Girolami, *Organometallics*, 1996, **15**, 5359; (*c*) C. L. Gross, J. L. Brumaghim and G. S. Girolami, *Organometallics*, 2007, **26**, 2258.
18 G. J. Perkins, M. I. Bruce, B. W. Skelton and A. H. White, *Inorg. Chim. Acta*, 2006, **359**, 2644.
19 J. L. Brumaghim and G. S. Girolami, *Chem. Commun.*, 1999, 953.
20 P. W. Wanandi and T. D. Tilley, *Organometallics*, 1997, **16**, 4299.
21 P. B. Glaser, P. W. Wanandi and T. D. Tilley, *Organometallics*, 2004, **23**, 693.
22 J. L. Brumaghim, C. L. Cross and G. S. Girolami, *J. Organomet. Chem.*, 2006, **691**, 3874.
23 G. J. H. va Nes and A. Vos, *Acta Crystallogr., Sect. B*, 1978, **34**, 1947.
24 G. J. H. va Nes and A. Vos, *Acta Crystallogr., Sect. B*, 1979, **34**, 2580.
25 (*a*) S. Szafert and J. A. Gladysz, *Chem. Rev.*, 2003, **103**, 4175; (*b*) S. Szafert and J. A. Gladysz, *Chem. Rev.*, 2006, **106**, PR1.
26 R. D. Shannon, *Acta Crystallogr., Sect. A*, 1976, **32**, 751.
27 (*a*) G. Frapper and M. Kertesz, *Inorg. Chem.*, 1993, **32**, 732; (*b*) N. Re, A. Sgamellotti and C. Floriani, *J. Chem. Soc., Dalton Trans.*, 1998, 2521; (*c*) N. Ouddaï, K. Costuas, M. Bencharif, J.-Y. Saillard and J.-F. Halet, *C. R. Chim.*, 2005, **6**, 1336.
28 C. Creutz, *Prog. Inorg. Chem.*, 1983, **30**, 1.
29 W. Kaim and G. K. Lahiri, *Angew. Chem., Int. Ed.*, 2007, **46**, 1778.
30 W. Henderson, J. S. McIndoe, B. K. Nicholson and P. J. Dyson, *J. Chem. Soc., Dalton Trans.*, 1998, 519.
31 M. Krejcik, M. Danek and F. Hartl, *J. Electroanal. Chem.*, 1991, **317**, 179.
32 C. M. Fendrick, E. H. Mintz, L. D. Schertz, T. J. Marks and V. M. Day, *Organometallics*, 1984, **3**, 819.
33 A. B. Holmes and C. N. Sporikou, *Org. Synth.*, 1987, **65**, 61.
34 G. E. Jones, D. A. Kendrick and A. B. Holmes, *Org. Synth.*, 1993, **Coll. Vol. 8**, 63.
35 N. G. Connelly and W. E. Geiger, *Chem. Rev.*, 1996, **96**, 877.
36 *The XTAL 3.7 System*, ed. S. R. Hall, D. J. du Boulay and R. Olthof-Hazekamp, University of Western Australia, Crawley, Australia, 2000.
37 (*a*) G. te Velde, F. M. Bickelhaupt, C. Fonseca Guerra, S. J. A. van Gisbergen, E. J. Baerends, J. G. Snijders and T. Ziegler, *J. Comput. Chem.*, 2001, **22**, 931; (*b*) C. Fonseca Guerra, J. G. Snijders, G. te Velde and E. J. Baerends, *Theor. Chem. Acc.*, 1998, **99**, 391; (*c*) *ADF2005, Theoretical Chemistry*, Vrije Universiteit, Amsterdam, The Netherlands, 2005SCM.
38 S. D. Vosko, L. Wilk and M. Nusair, *Can. J. Chem.*, 1990, **58**, 1200.
39 (*a*) A. D. Becke, *Phys. Rev. A: At., Mol., Opt. Phys.*, 1988, **38**, 3098; (*b*) J. P. Perdew, *Phys. Rev. B*, 1986, **33**, 8822.
40 L. Verluis and T. Ziegler, *J. Chem. Phys.*, 1988, **88**, 322.
41 (*a*) E. van Lenthe, E. J. Baerends and J. G. Snijders, *J. Chem. Phys.*, 1993, **99**, 4597; (*b*) E. van Lenthe, E. J. Baerends and J. G. Snijders, *J. Chem. Phys.*, 1994, **101**, 9783; (*c*) E. van Lenthe, R. van Leeuwen, E. J. Baerends and J. G. Snijders, *Int. J. Quantum Chem.*, 1996, **57**, 281.
42 S. J. A. van Gisbergen, J. G. Snijders and E. J. Baerends, *Comput. Phys. Commun.*, 1999, **118**, 119.